Neuropathology of white matter lesions, blood-brain barrier dysfunction and dementia

Atticus H Hainsworth PhD[1,2,3*], Thais Minett PhD[4,5], Joycelyn Andoh BSc[1,3], Gillian Forster MSc[6], Ishaan Bhide MBBS[1,3], Thomas R Barrick PhD[3], Kay Elderfield MSc[7], Jamuna Jeevahan MSc[7], Hugh S Markus DM, FRCP[8], Leslie R Bridges MD, FRCPath[1,3,7]

[1]Cell Biology and Genetics Research Centre, Molecular and Clinical Sciences Research Institute, St Georges University of London, London, UK.

[2]Neurology, St George's University Hospitals NHS Foundation Trust, Blackshaw Road, London, UK.

[3]Neuroscience Research Centre, Molecular and Clinical Sciences Research Institute, St Georges University of London, London, UK.

[4]Department of Public Health and Primary Care, University of Cambridge, UK

[5]Department of Radiology, University of Cambridge, UK

[6]The Sheffield Institute for Translational Neuroscience, University of Sheffield, UK

[7]Department of Cellular Pathology, St George's University Hospitals NHS Foundation Trust, London.

[8] Stroke Research Group, Department of Clinical Neurosciences, University of Cambridge, UK.

[*]**Correspondence**: Dr Atticus Hainsworth, Mailpoint J-0B, St Georges University of London, Cranmer Terrace, London, SW17 0RE, United Kingdom. Tel +44 208 725 5586, Fax +44 208 725 2950, email ahainsworth@sgul.ac.uk

Running title: BBB pathology and dementia [26 characters <40]

Supplementary Methods

Diagnosis of Dementia

Dementia status at death for each participant was determined by combining all information available, including: i) assessments during the last years of life, ii) informant interviews after death, iii) death certificates. A study diagnosis of dementia was made if: dementia was present at any assessment, based on the full GMS AGECAT diagnostic algorithm[1] (equivalent to DSM-IIIR); or if dementia was noted on the death certificate; or if a detailed retrospective interview with a knowledgeable informant, covering the diagnostic domains required for clinical diagnosis including separation from terminal decline, indicated that dementia was present. Participants were considered to have died without dementia if: they did not have dementia at their last interview and that interview had been conducted less than six months before death; or if they did not have dementia at their last interview and the retrospective interview indicated no dementia at death[2].

APOE genotype was available for 108 participants. At least one *APOE2* allele was present in 19 (15%), and at least one *APOE4* in 33 (26%) individuals.

Neuropathological Assessment of MRC-CFAS brain tissue

Pathological evaluation of the MRC CFAS cohort has been described in detail previously[2-4]. Assessments of plaques, CAA and tangles, were conducted by neuropathologists blinded to clinical data, using immunohistochemical and tinctorial methods. The severity of amyloid plaques and CAA were scored semi-quantitatively according to the Consortium to Establish a Registry for Alzheimer's Disease (CERAD) protocol[4, 5] as either 'none', 'mild', 'moderate' or 'severe'. As the score 'severe' was infrequent, data were dichotomised for analysis to "none-mild" and 'moderate-severe'. Neurofibrillary tangle pathology was rated according to the Braak and Braak staging 0-VI[6, 7] and partitioned into three subgroups: 0-II, III-IV and V-VI.

Post Mortem MRI Scanning

For all brains sampled, one cerebral hemisphere was fixed in 10% buffered formaldehyde for a minimum of four weeks and then cut into 10 mm coronal slices ("thick slices"). Thick slices were selected at three levels (Newcastle Brain Map coronal reference levels 10/12, 19/20, 24/25)[8, 9]. Thick slices were sealed in polythene bags then placed caudal-side up in a custom-built 'self-locking' stack designed to fit the knee coil of an MRI scanner[10]. MRI was performed with a 1.0 T scanner (Siemens, Munich, Germany) using pulse sequences previously optimized for studying post-mortem white matter hyperintensities (WMH)[10, 11]. For all sequences, a single MRI image was obtained at the centre of the thick slice by positioning a 5-mm window individually, with an in-plane resolution of 0.63 mm x 0.59 mm. MRI scans were rated by consensus by three experienced observers, blinded to clinical and neuropathological information[10]. Scans of thick slices from the same brain were arranged nonconsecutively to reduce potential bias.

All WMH were marked by hand on a diagram of the MRI scans, to guide histological sampling of white matter tissue blocks from thick slices, as described[10, 11]. See Supplementary Figure I, below. WMH were classified into "deep subcortical" and "periventricular" and scored using a modification of a protocol developed for in vivo scanning[12]. The number and size of the WMH were rated in hard copies of the scans according to the largest diameter of the WMH in each slice[10-12].

Among the 151 tissue blocks sampled, 69 were from a thick slice with no MRI-defined WMH; 18 were from thick slices with sub-cortical WMH up to 10 mm in greatest diameter and up to 10 in number; 64 were from thick slices with sub-cortical WMH >11 mm in diameter, or confluent WMH.

Primary antibodies

Human fibrinogen (rabbit polyclonal A-0080), and human IgG primary antibodies (rabbit polyclonal A-0423) were from Dako-Cytomation, Ely, Cambs., UK. Human IgG monoclonal antibody (mouse IgG_1, Clone RWP49) was from Novocastra-Leica Microsystems, Newcastle-upon-Tyne, UK, and the immunogen was a recombinant protein corresponding to 327 residues of human IgG. All these antibodies have been characterised previously[13]. Human CD68 (mouse monoclonal antibody, clone PGM1) was from Dako-Cytomation, Ely, UK and has been characterised previously[10].

Histopathology and Immunohistochemistry

Endogenous peroxidase activity was blocked by exposure to H_2O_2 (3% v/v, aqueous solution) for 8 min. After high-pressure heat-induced antigen retrieval (30 s, 125 ^oC, in pH 7.8 Tris-citrate buffer), non-specific binding was blocked with phosphate buffered saline containing 0.1 % v/v Triton-X100 and 3 % (w/v) bovine serum albumin (PBT-BSA) for 60 min at room temperature. Sections were then exposed to primary antibodies at 4 ^oC overnight.

Neighbouring sections from each tissue block were labelled for fibrinogen or for the activated microglial marker CD68 (PGM1). Additional markers used were human IgG, GFAP and AQP4. Primary antibodies were diluted on the day of use in PBT-BSA. Primary antibodies were fibrinogen (diluted 1:30,000), polyclonal IgG (1:100,000), monoclonal IgG (1:400), CD34 (1:100), SMA (1:600) and monoclonal CD68-PGM1 (1:400). Antibody labelling was visualised using a peroxidase-conjugated secondary reagent (Envision® kit, K4065, Dako, Carpinteria, CA) and diaminobenzidine (DAB) chromagen, then counterstained with Mayer's haematoxylin. As a negative control neighbouring sections were treated identically with an irrelevant primary antibody (rabbit polyclonal anti-sheep IgG; BD-Pharmingen).

Digital Histology and Image Analysis

All histochemical labelling and image analysis was performed blind to clinical and MRI data. All sections were digitally scanned under a 20x objective lens (Leica Slidescanner, accessed via UCL-Advanced Diagnostics). Scanned sections were stored as .scn files, and viewed using Leica Slidepath Gateway free software (www.leicabiosystems.com/).

For each fibrinogen labelled section and each CD68 labelled section, a single blinded observer (JA) sampled 5 images at 10x magnification (each image area 0.967 mm^2) according to a pre-determined, geometric sampling protocol. Based on the approximately rectangular form of each tissue section, images were sampled from the centroid of the white matter area and 4 images distributed orthogonally around the centroid (total sampled area per section: 4.84 mm^2).

Additionally, for each section containing a histopathology-defined lesion, the .scn files for CD68 and neighbouring fibrinogen labelled sections were co-registered within Leica Slidepath Gateway software (aligned as in the examples in Supplementary Figure II). Non-overlapping images at 10x

magnification (each image area 0.967 mm^2) were then sampled from the co-registered sections, so as to cover the full extent of each cluster of CD68 positive amoeboid microglia.

All sampled images were then fed into a threshold detection algorithm within NIH ImageJ free software (http://imagej.nih.gov/ij) to determine fgen_AF and CD68_AF. Labelled pixels were detected using a fixed threshold detection method. An inbuilt maximum entropy filter was applied to all images to minimise bias in the area fraction measurements. The labelled area fraction was expressed as 100 x (number of positive pixels/total pixels).

Following completion of the histological analysis we were unblinded to MRI status for each tissue sample, and fgen_AF and CD68_AF were analysed statistically by tissue type. For tissue sections derived from an MRI-defined WMH, and containing a histopathology-defined lesion, we used fgen_AF and CD68_AF data that had been obtained from CD68-directed sampling of co-registered images. For all other tissue types, we used fgen_AF and CD68_AF data derived from geometric sampling of images.

Supplementary Figures

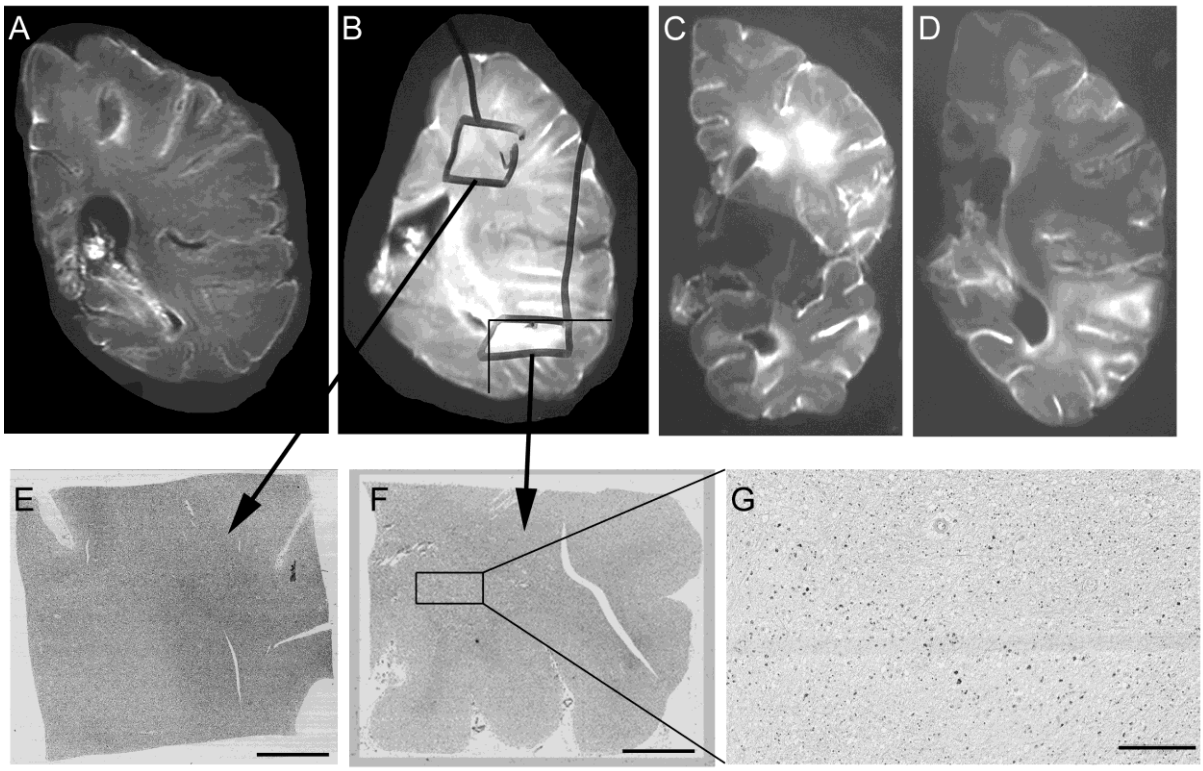

Supplementary Figure I. Examples of post mortem MRI scans of thick coronal slices from three different participants (upper row). A, MRI-normal brain, with no WMH detected. B, WMH-containing brain, showing mark-up of tissue areas on the MRI scan, for sampling NAWM and WMH. C, another WMH-containing brain, following tissue sampling of a WMH area. D, different slice from the same brain as C, without mark-up or sampling. E, NAWM tissue block from harvested from the thick slice in B. F, WMH tissue block from B. G, CD68-labelled histological section from F, showing a histological lesion. Scale bars 5 mm in E and F, 100 µm in G.

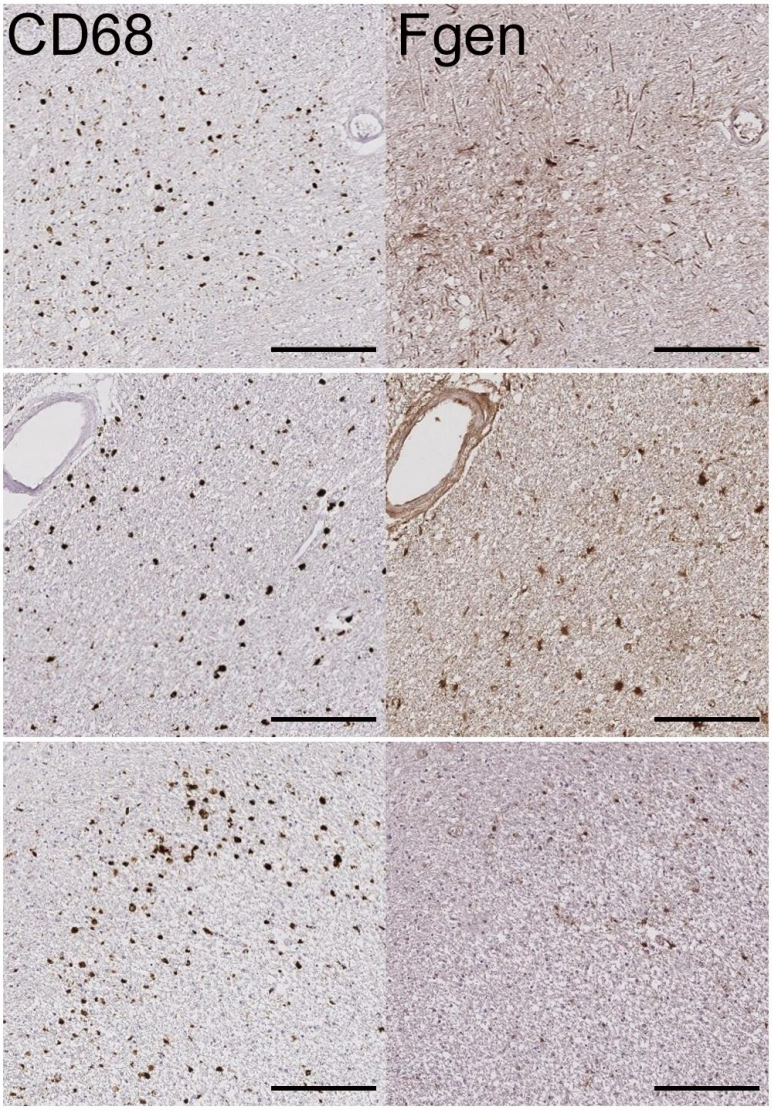

Supplementary Figure II. Examples of histopathology-directed image sampling in subcortical white matter.

CD68 (PGM1)-labelled sections (left column) show clusters of amoeboid microglia, defined as histological white matter lesions. Neighbouring sections labelled with fibrinogen (right column) were co-registered within Slidepath Gateway software. Fibrinogen positive cells and axons are evident in the upper two panels. Scale bars 200 µm.

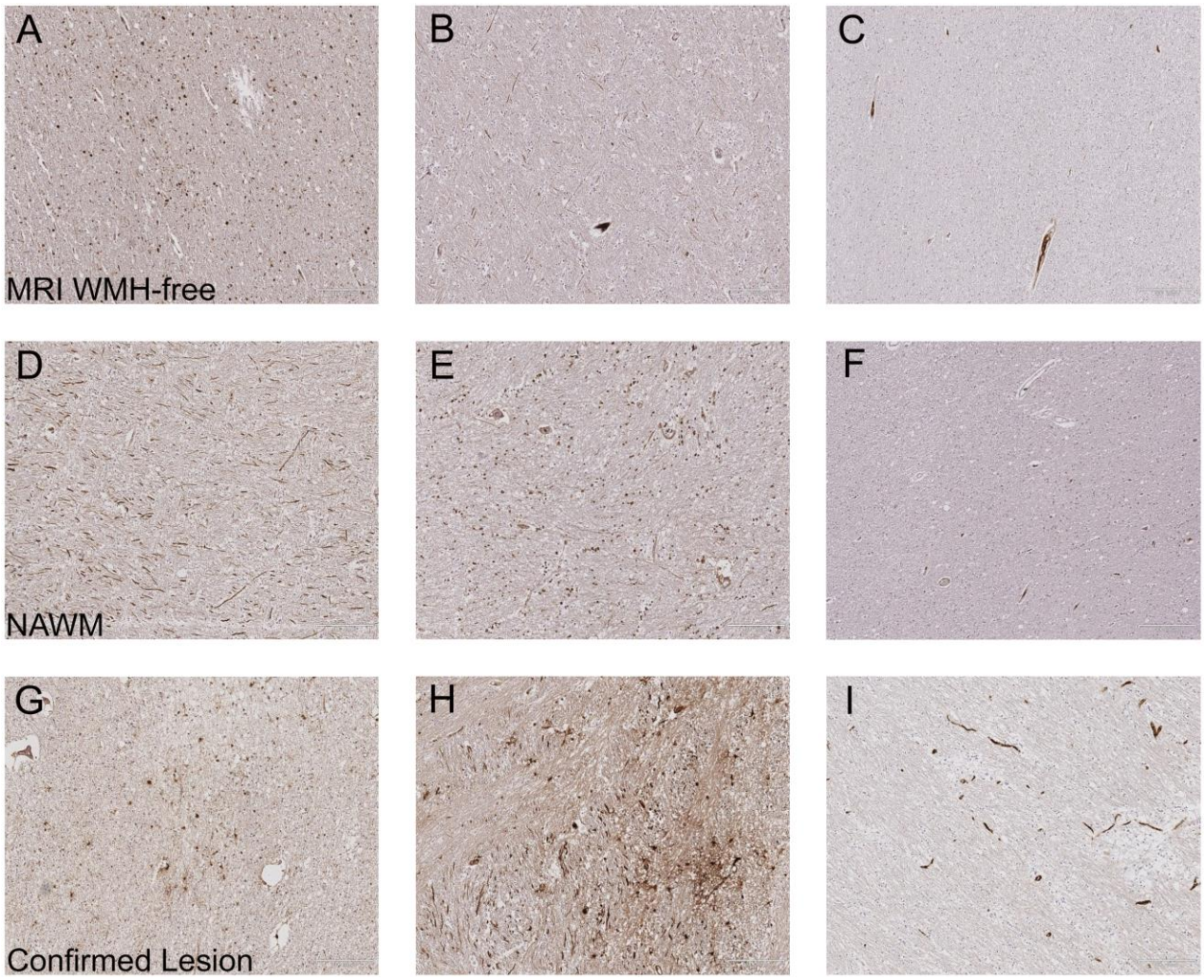

Supplementary Figure III. Fibrinogen-labelled subcortical white matter tissue, examples of three tissue types: healthy (WMH-free) white matter, normal-appearing white matter (NAWM) and WMH confirmed as white matter lesions by CD68-PGM1 immunohistochemistry (Confirmed Lesion).

Tissue blocks were derived from MRI WMH-free brains (A-C), or from brains containing WMH (D-I). Panels D-F show NAWM and G-I show MRI-defined WMH containing CD68-defined lesions. Fibrinogen positive cellular labelling was present in all tissue types (A-B, D-E and G-H). Likewise, tissue sections lacking fibrinogen cellular labelling were seen in all three tissue types (C, F, I). Intra-vascular labelling confirms antigenicity (C, F, I). Scale bars 200 µm.

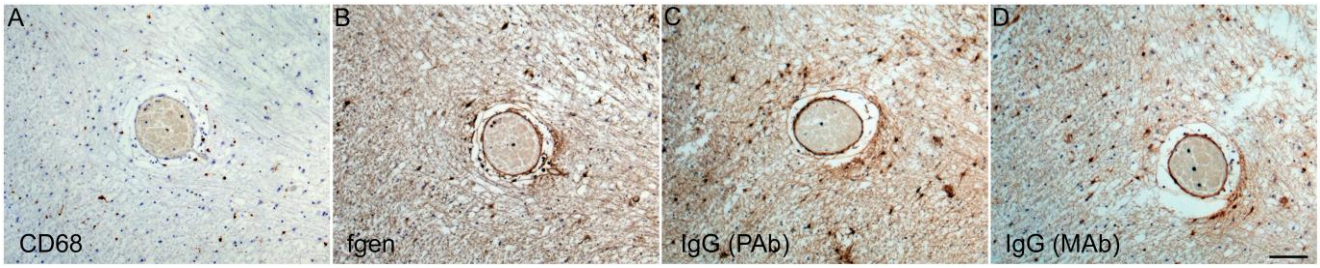

Supplementary Figure IV. Immunohistochemical labelling with fibrinogen compared with IgG and CD68 in subcortical white matter.

Neighbouring sections from the same tissue block, around a landmark vessel (small vein). Sections were immunolabelled either for CD68-PGM1 (panel A) or for fibrinogen (fgen, panel B) or for immunoglobulin G (IgG, panels C and D). Immunolabelling for IgG (polyclonal or monoclonal antibodies, panels C, D respectively) gives a similar labelling pattern to fibrinogen (B). Extra-vascular labelling, including cellular labelling, is seen in B, C and D. Scale bar 100 µm.

Supplementary Table I. Relationship between the presence of white matter abnormality and fibrinogen immunolabelling

	Fibrinogen area fraction		
	β	95% CI (β)	p
*MRI-defined WMH**			
• MRI: NAWM	-0.16	(-0.41; 0.10)	0.229
• MRI: WMH	-0.09	(-0.33; 0.15)	0.451
*Histology-defined white matter lesions***			
• Histological lesion	-0.02	(-0.20; 0.16)	0.827
*Combined method****			
• MRI NAWM, histology non-lesion	-0.07	(-0.34; 0.20)	0.613
• MRI WMH, histology non-lesion	-0.07	(-0.33; 0.18)	0.571
• MRI: normal or NAWM, histology lesion	-0.20	(-0.63; 0.24)	0.370
• MRI WMH, histology lesion	-0.03	(-0.31; 0.26)	0.845

*reference: MRI WMH-free brains. **reference: histopathology non-lesion white matter. ***reference: MRI WMH-free, histopathology non-lesion

Weighted linear regression analyses were performed with MRI classification (MRI normal, NAWM, WMH) as independent variable and fibrinogen area fraction as dependent variable. The same analyses were repeated with histologically (CD68)-defined WML (none, present) as independent variable and also with combined MRI/histological methods.

Abbreviations. WMH: white matter hyperintensity. NAWM: normal-appearing white matter.

Supplementary Reference List

(1) Copeland JR, Dewey ME, Griffiths-Jones HM. A computerized psychiatric diagnostic system and case nomenclature for elderly subjects: GMS and AGECAT. *Psychol Med.* 1986;16:89-99.

(2) Savva GM, Wharton SB, Ince PG, Forster G, Matthews FE, Brayne C. Age, neuropathology, and dementia. *N Engl J Med.* 2009;360:2302-2309.

(3) MRC-CFAS. Pathological correlates of late-onset dementia in a multicentre, community-based population in England and Wales. Neuropathology Group of the Medical Research Council Cognitive Function and Ageing Study (MRC CFAS). *Lancet.* 2001;357:169-175.

(4) Richardson K, Stephan BC, Ince PG, Brayne C, Matthews FE, Esiri MM. The neuropathology of vascular disease in the Medical Research Council Cognitive Function and Ageing Study (MRC CFAS). *Curr Alzheimer Res.* 2012;9:687-696.

(5) Mirra SS, Heyman A, McKeel D, Sumi SM, Crain BJ, Brownlee LM et al. The Consortium to Establish a Registry for Alzheimer's Disease (CERAD). Part II. Standardization of the neuropathologic assessment of Alzheimer's disease. *Neurology.* 1991;41:479-486.

(6) Braak H, Braak E. Neuropathological stageing of Alzheimer-related changes. *Acta Neuropathol.* 1991;82:239-259.

(7) Nelson PT, Alafuzoff I, Bigio EH, Bouras C, Braak H, Cairns NJ et al. Correlation of Alzheimer disease neuropathologic changes with cognitive status: a review of the literature. *J Neuropathol Exp Neurol.* 2012;71:362-381.

(8) Perry RH, Oakley AE. *Newcastle Brain Map*. London,UK: Wolfe; 1993.

(9) Kalaria RN. Neuropathological diagnosis of vascular cognitive impairment and vascular dementia with implications for Alzheimer's disease. *Acta Neuropathol.* 2016;131:659-685.

(10) Fernando MS, O'Brien JT, Perry RH, English P, Forster G, McMeekin W et al. Comparison of the pathology of cerebral white matter with post-mortem magnetic resonance imaging (MRI) in the elderly brain. *Neuropathol Appl Neurobiol.* 2004;30:385-395.

(11) Fernando MS, Simpson JE, Matthews F, Brayne C, Lewis CE, Barber R et al. White matter lesions in an unselected cohort of the elderly: molecular pathology suggests origin from chronic hypoperfusion injury. *Stroke.* 2006;37:1391-1398.

(12) Scheltens P, Barkhof F, Leys D, Pruvo JP, Nauta JJ, Vermersch P et al. A semiquantative rating scale for the assessment of signal hyperintensities on magnetic resonance imaging. *J Neurol Sci.* 1993;114:7-12.

(13) Bridges LR, Andoh J, Lawrence AJ, Khoong CH, Poon WW, Esiri MM et al. Blood-brain barrier dysfunction and cerebral small vessel disease (arteriolosclerosis) in brains of older people. *J Neuropathol Exp Neurol.* 2014;73:1026-1033.